


Article

Facile Synthesis of PtPd Network Structure Nanochains Supported on Multi-Walled Carbon Nanotubes for Methanol Oxidation

Dawei Zhang ^{1,†}, Yanrong Ren ^{2,†}, Zhenhua Jin ², Yonghua Duan ¹, Mingli Xu ² and Jie Yu ^{1,*} ¹ Faculty of Materials Science and Engineering, Kunming University of Science and Technology, Kunming 650093, China² Faculty of Metallurgical and Energy Engineering, Kunming University of Science and Technology, Kunming 650093, China

* Correspondence: yujie@kust.edu.cn

† These authors contributed equally to this work.

Abstract: In this paper, a PtPd NC catalyst with a network structure of nanochains was prepared with KBr as a structure-directing agent, NaBH₄ as a reducing agent, and modified multi-walled carbon nanotubes (MWCNTs) as a support. The experimental results show that the structure-directing agent KBr helps to form a particular type of nanochain with a network topology. PtPd NCs with various ratios (Pt:Pd = 2:1, 1:1, 1:2) have respective diameters of 30 nm, 35 nm, and 23 nm. With numerous structural flaws at the junctions, the nanochains' distinctive network structure increases the number of active sites on the PtPd nanocenter surface. Electrochemical characterization results show that the current density of the PtPd NCs is about 658.5 mA mg^{−1}, 1.5-times that of the Pt/C catalyst and 3.9-times that of the commercial Pd/C catalyst. Furthermore, it has better electrocatalytic stability for methanol oxidation than Pd/C and Pt/C catalysts.

Keywords: network structure; platinum–palladium nanochains; methanol; structural defects; electrocatalysis



Citation: Zhang, D.; Ren, Y.; Jin, Z.; Duan, Y.; Xu, M.; Yu, J. Facile Synthesis of PtPd Network Structure Nanochains Supported on Multi-Walled Carbon Nanotubes for Methanol Oxidation. *Metals* **2022**, *12*, 1911. <https://doi.org/10.3390/met12111911>

Academic Editors: Yuhong Zhao, Junsheng Wang and Renhai Shi

Received: 12 October 2022

Accepted: 4 November 2022

Published: 8 November 2022

Publisher's Note: MDPI stays neutral with regard to jurisdictional claims in published maps and institutional affiliations.



Copyright: © 2022 by the authors. Licensee MDPI, Basel, Switzerland. This article is an open access article distributed under the terms and conditions of the Creative Commons Attribution (CC BY) license (<https://creativecommons.org/licenses/by/4.0/>).

1. Introduction

Direct methanol fuel cells (DMFCs) have received many researchers' extensive attention due to their high energy density, high conversion efficiency, and environmental friendliness [1,2]. Additionally, due to the abundant supply of methanol, simplicity of storage, and accessibility of current fuel delivery systems, DMFCs have become extremely attractive [3–5]. However, the kinetic process of the methanol oxidation reaction at the DMFC anode is so slow that it produces incomplete oxidation intermediates, such as CO, and these intermediates will make adsorption on the catalyst surface and cover the active site, which will eventually lead to a reduction in catalyst activity. On the other hand, the catalyst will dissolve in the electrolyte during the catalytic process, which will lead to the instability of the whole cell system and affect the service life. Therefore, the development of DMFC catalysts with high catalytic performance and high stability is beneficial for the practical application of DMFCs [6–8].

Compared with the single metal catalysts, Pt/Pd-based catalysts have better stability and catalytic activity [9–13], thus, enhancing the anti-poisoning ability of the catalysts. Studies have shown that special morphologies of PtPd bimetallic nanostructured catalysts present excellent catalytic performance for DMFCs due to the synergistic effect and electronic interaction between Pt and Pd atoms [14,15].

The activity of the catalyst is closely related to its morphology, structure, and particle size [16–21]. Yizhong Lu et al. [22] successfully synthesized PtPd porous nanorods through a bromide-induced galvanic replacement reaction between Pd nanowires and K₂PtCl₆.

Chunmei Zhang [23] prepared a PtPd alloy with concave nanocubes via a hydrothermal reaction in the presence of GO. Dong and his colleagues [24] used Te nanowires as corrosion templates and reducing agents to prepare AuPtPd nanowires. Guo et al. synthesized Te nanowires via the hydrothermal method, then synthesized Pd nanowires with Te nanochains as a reducing agent and template and, finally, synthesized PtPd nanowires using ascorbic acid as a reducing agent precursor. Achari I. prepared an ultra-thin $Pt_xPd_{(1-x)}$ alloy catalyst by the low potential deposition of a H sacrificial layer surface, restricting redox replacement [25]. However, the reaction time required by the above-synthesized methods is relatively long and the reaction process is very complicated. In addition, these organic structure-directing agents may also hinder the reaction's mass transfer or electron transfer, thus, seriously limiting the practical application of the catalysts. Among various morphologies of PtPd nanocatalysts, PtPd nanochains have a unique network structure [26,27] with a large specific surface area and more active sites that can be used as highly efficient fuel cell catalysts. Multi-walled carbon nanotubes (MWCNTs) have many advantages, such as large specific surface area, good electrical conductivity, and a high degree of crystallization [28–30]. MWCNTs are often used as support for nanoparticles because it is conducive to improving the utilization of precious metals and enhancing the interaction between carriers and noble metal nanoparticles.

In this paper, we use the inorganic reagent potassium bromide as a structure-directing agent to synthesize a PtPd NC catalyst with a network structure at room temperature by a simple one-step chemical reduction method. The morphology, structure, and particle size with electrocatalytic performance were discussed for the synergistic interaction between Pt and Pd.

2. Experiments

2.1. Chemical Agents

The chemical reagents used are as follows: palladium chloride (II) ($PdCl_2$), potassium chloroplatinate (II) (K_2PtCl_6), polyethylene glycol (PEG-400), potassium bromide (KBr), multi-walled carbon nanotubes (MWCNTs), potassium hydroxide (KOH), sodium borohydride ($NaBH_4$), isopropanol, methanol, nafion solution (5 wt%), deionized water (18.25 MΩ cm). All aqueous solutions were prepared with twice-distilled water.

2.2. Preparation of PtPd NCs/MWCNTs

Firstly, 24 mL PEG, 1 mL K_2PtCl_6 (2.34 mg mL^{−1}), and 4 mL Na_2PdCl_4 (0.325 mg mL^{−1}) were evenly mixed with 1 mL KBr (0.1 mol L^{−1}). Secondly, 50 mL fresh $NaBH_4$ (0.48 mol L^{−1}) was added into the above-mixed solution drop by drop under stirring, then Pt_1Pd_1 NCs were obtained after 50 min of reaction under magnetic stirring. The above colloidal solution was added to the previously modified and ultrasonically dispersed MWCNTs (Section 2.1 of the study [4] as the modification method). After stirring for 4 h, Pt_1Pd_1 NC/MWCNT catalyst was obtained by filtration and washed with deionized water then dried at 60 °C for 12 h. With the same method as above, Pt_1Pd_2 NCs/MWCNTs and Pt_2Pd_1 NCs/MWCNTs were synthesized by Pt:Pd metal molar ratio of 1:2 and 2:1, respectively. For comparison, PtPd nanoparticles were also synthesized without structure-directing agent KBr with the same method as the above PtPd NPs.

2.3. Physical Characterization

A transmission electron microscope (TEM, Tecnai G2 F20 S-Twin) (FEI, Hillsboro, OR, USA) was used to test the morphology and dispersion of the noble metal nanoparticles operated at 200 kV. A powder X-ray diffractometer (XRD, Rigaku miniFlex600 powder diffractometer) was used to characterize the sample's crystal phase structure and crystal grain size. Diffraction peaks were collected from 10° to 90° (2θ) at a sweep speed of 2° min^{−1}. EDS was used to analyze the elements of the catalysts. The chemical components of every element were collected on X-ray Photoelectron spectra (XPS, Thermo K-Alpha⁺) with a monochromatic aluminum Kα (1486.6 eV) X-ray source operating at 150 W.

2.4. Electrochemical Measurements

All electrochemical measurements were performed using a three-electrode system with the CHI660C electrochemical workstation, the glassy carbon electrode as the working electrode, the platinum electrode as the counter electrode, and the saturated calomel electrode (Ag/AgCl) as the reference electrode. The surface of the glassy carbon electrode with a 3 mm diameter was polished to a mirror surface by using Al_2O_3 with a diameter of 300 nm and 50 nm in succession, ultrasonically washed in ethanol for 3 min, rinsed with deionized water, and air-dried. Then, 950 μL of isopropanol and 50 μL of Nafion solution were ultrasonically mixed and 2 mg of the prepared catalyst was added and ultrasonicated for another 20 min to form an ink-like suspension. A 10 μL sample was dropped on the surface of a cleaned glassy carbon electrode using a micro-injector and allowed to air dry. The electrocatalytic activity and stability of the catalysts for methanol were tested in a 0.5 M KOH + 2 M CH_3OH solution (the N_2 is saturated with the solution for 20 min to remove dissolved oxygen). The electrochemical test temperature was 30 $^\circ\text{C}$, the scan range was $-0.8\sim 0.4$ V (vs. Ag/AgCl), and the scan rate was 50 $\text{mV}\cdot\text{s}^{-1}$.

3. Results and Discussion

3.1. Physicochemical Characterization

Figure 1A,B show the TEM images of Pd_1Pt_1 NCs at different magnification ratios (200 nm, 100 nm). The figures display a network structure and rough surface nanochains. This results in a higher specific surface area and more active sites so as to improve catalytic performance. The structural characteristics of $\text{Pt}_1\text{Pd}_1\text{NCs}$ are further analyzed by HRTEM. Figure 1C shows that $\text{Pt}_1\text{Pd}_1\text{NCs}$ are connected by a stack of nanoparticles with a diameter of about 4.5 nm, easily distinguished by their crystalline interplanar spacing around 0.224 nm (the spacing of Pt and Pd is 0.226 nm and 0.2245 nm). Additionally, the nanoparticles in the nanochains display varying growth directions, which may help the nanochains to develop a network structure.

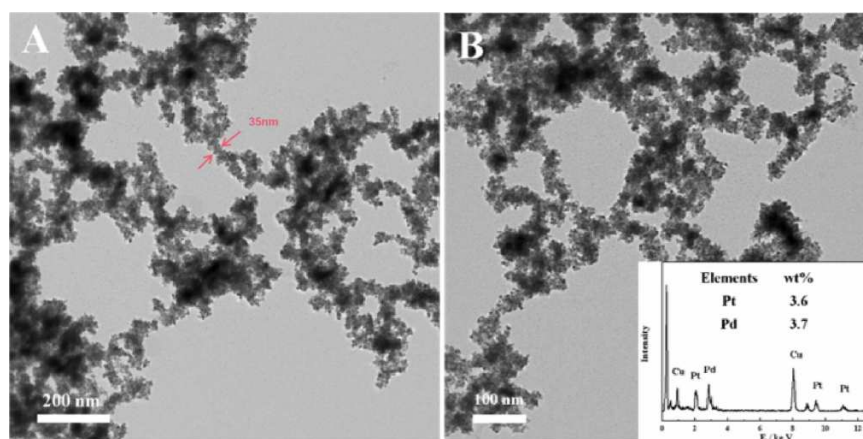


Figure 1. Cont.

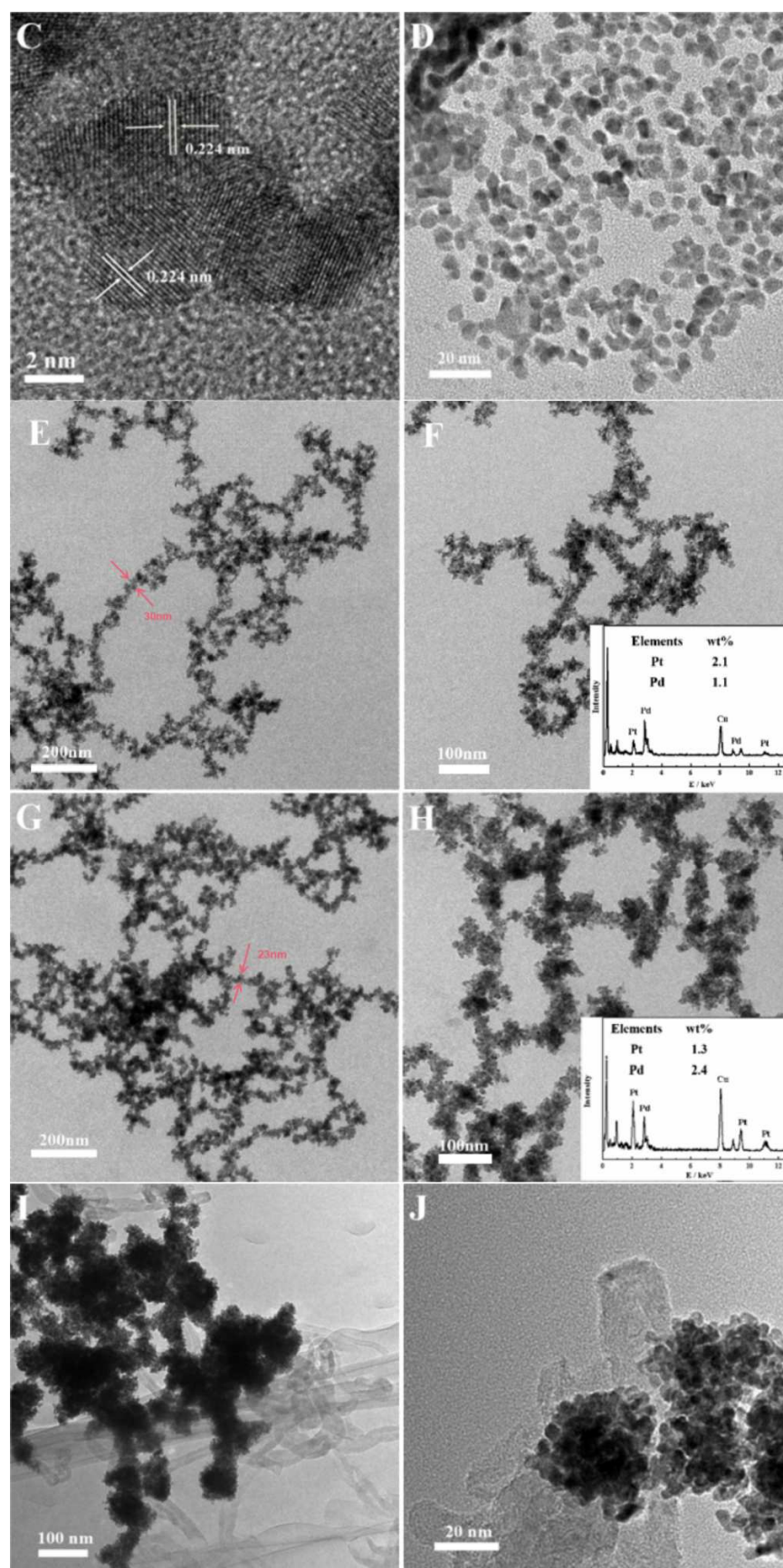


Figure 1. The TEM images and EDS of (A,B) Pt₁Pd₁ NCs, (C) the HRTEM image of Pt₁Pd₁ NCs, (D) Pt₁Pd₁ NPs (without KBr), (E,F) Pt₂Pd₁ NCs, (G,H) Pt₁Pd₂ NCs, (I,J) Pt₁Pd₂ NCs/MWCNTs.

Figure 1E–H are TEM images of Pt_2Pd_1 NCs and Pt_1Pd_2 NCs at different magnifications (200 nm, 100 nm), respectively. The network structure nanochain's average diameters for Pt_2Pd_1 NCs, Pt_1Pd_1 NCs, and Pt_1Pd_2 NCs are about 30 nm, 35 nm, and 23 nm, respectively, and the Pt_1Pd_2 NCs have the finest diameter. Because the reduction potential of Pd^{2+}/Pd (0.915 V) is less than that of Pt^{2+}/Pt (1.18 V), Pd may be reduced preferentially. With the increase in Pd content, the nucleation number of the nanoparticles will also increase. When the content of Pd is higher than Pt, the diameter of the nanoparticles becomes small and the nanochains become fine. As a result, tiny nanoparticles are linked together to form nanochains to provide a bigger specific surface area and more active sites, which is advantageous to increase the catalytic performance of the catalyst. For further determining the composition of the nanochains, EDS of Pt_2Pd_1 NCs, Pt_1Pd_1 NCs, and Pt_1Pd_2 NCs is analyzed. From Figure 1B,F,H (bottom right corner), the nanochains are composed of two elements, Pt and Pd, because the atomic percentage of Pt and Pd in each catalyst is consistent with the molar ratio of metal in the precursor solution, demonstrating that the metal ions in the solution are completely reduced.

Figure 1D shows a TEM image of Pt_1Pd_1 NPs without the structure-directing agent KBr for comparison. As Figure 1D shows, a large number of PtPd NPs nanoparticles have formed and there is no network structure. There may be two possible reasons: (1) Since Br^- has a strong chemisorption capacity, it is advantageous as a ligand to form $[\text{PdBr}_4]^-$ and $[\text{PtBr}_4]^-$ complexes in PEG-400 with a helical structure [29]. As a protective agent, it is quickly reduced to fine nanoparticles. (2) Br^- can easily combine with the (100) plane of the face-centered cubic crystal structure of the metal to suppress the growth of the (100) crystal plane and Br^- has an etching effect. They jointly lead to the formation of a network structure of PtPd network structure nanochains. In addition, Figure 1I,J show that the Pt_1Pd_2 NCs are uniformly supported on the surface of MWCNTs. It is advantageous to increase the specific surface area, form more active sites, and enhance the electrocatalytic performance.

XRD spectra of three as-synthesized PtPd NCs/MWCNTs catalysts are shown in Figure 2. The diffraction angles $20.39.9^\circ$, 46.4° , 67.8° , and 81.6° , which correspond to the (111), (200), (220), and (311) crystal planes of Pt and Pd, respectively, certify that the synthesized nanochains are a face-centered cubic structure [31]. The diffraction peaks of Pt_2Pd_1 NCs/MWCNTs, Pt_1Pd_1 NCs/MWCNTs, and Pt_1Pd_2 NCs/MWCNTs located between the standard peaks of Pt (JCPDS No. 04-0802) and Pd (JCPDS No. 46-1043) indicate that Pt and Pd form an alloy structure. As the Pd content increases, the diffraction peak shifts toward the standard peak of Pd, but the trend is not particularly noticeable. This may be because the lattice constants of Pt and Pd are very close, resulting in an insignificant shift tendency.

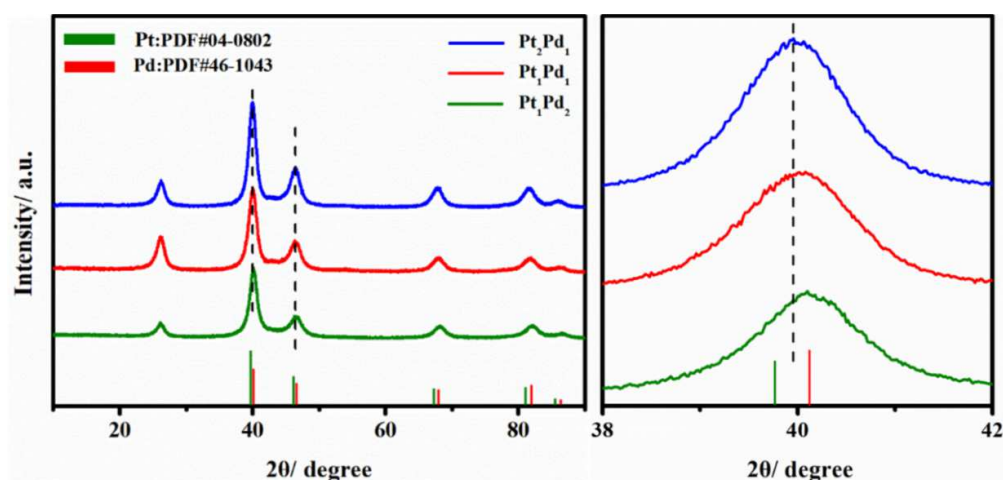


Figure 2. XRD patterns of Pt_2Pd_1 NCs/MWCNTs, Pt_1Pd_1 NCs/MWCNTs and Pt_1Pd_2 NCs/MWCNTs.

In order to describe the electronic structure of Pt and Pd in PtPd NCs affected by different molar ratios, the XPS spectra of Pt 4d and Pd 3d of three proportions of PtPd NCs are compared and the electrons corresponding to Pt 4f and Pd 3d are combined. The energy values are listed in Table 1. Figure 3A shows the Pt 4f spectra of Pt₁Pd₂ NCs with two major peaks at 71.4 and 74.7 eV for metallic Pt 4f_{7/2} and 4f_{5/2}, respectively, while other peaks at 72.3 and 75.2 eV show the oxidized form of Pt. Figure 3B shows the Pd 3d spectrum of Pt₁Pd₂ NCs, the two main peaks at 335.2 and 341.1 eV correspond to Pd(0), while the other peaks at 336.30 eV and 342.11 eV show the oxidized form of Pd. Based on the peak areas, it is known that Pt(0) and Pd(0) are mainly present in Pt₁Pd₂ NCs. Figure 3C is a Pt 4f spectrum of Pt₁Pd₁ NCs, Pt₂Pd₁ NCs, Pt₁Pd₂ NCs, and Pt NCs. For the Pt 4f 7/2 and Pt 4f 5/2 orbits of the Pt NCs catalyst, the electron-binding energies are 71.34 eV and 74.88 eV, respectively. As the Pt ratio of the nanochains decreases, compared with the Pt NCs, the offset of Pt₂Pd₁ NCs is maximum and the electron-binding energies of Pt 4f 7/2 and Pt 4f 5/2 are shifted to 0.52 eV and 0.67 eV, respectively. Figure 3D shows the Pd 3d spectra of Pt₁Pd₁ NCs, Pt₂Pd₁ NCs, Pt₁Pd₂ NCs, and Pd NCs. For the Pd 3d 5/2 and Pd 3d 3/2 orbits of the Pd NC catalyst, the electron-binding energy is 335.74 eV and 341.24 eV, respectively. Compared with Pd NCs, Pt₂Pd₁ NCs have the largest offset and the electron-binding energies of Pd 3d 5/2 and Pd 3d 3/2 are negatively shifted by 0.67 eV and 0.81 eV, respectively. The offset may be due to the internal electron transfer between Pt and Pd, resulting in a synergistic effect. This feature has a significant impact on the catalytic performance of PtPd NCs. In addition, it also proves that Pt and Pd form an alloy, which is consistent with the XRD results.

Table 1. Value of binding energies of Pt and Pd.

Samples	Pt 4f _{7/2}	Pt 4f _{5/2}	Pd 3d _{5/2}	Pd 4d _{3/2}
Pt	71.34	74.88	-	-
Pt:Pd = 2:1	70.82	74.21	335.07	340.43
Pt:Pd = 1:1	71.18	74.44	335.22	340.60
Pt:Pd = 1:2	71.16	74.41	335.43	340.78
Pd	-	-	335.74	341.24

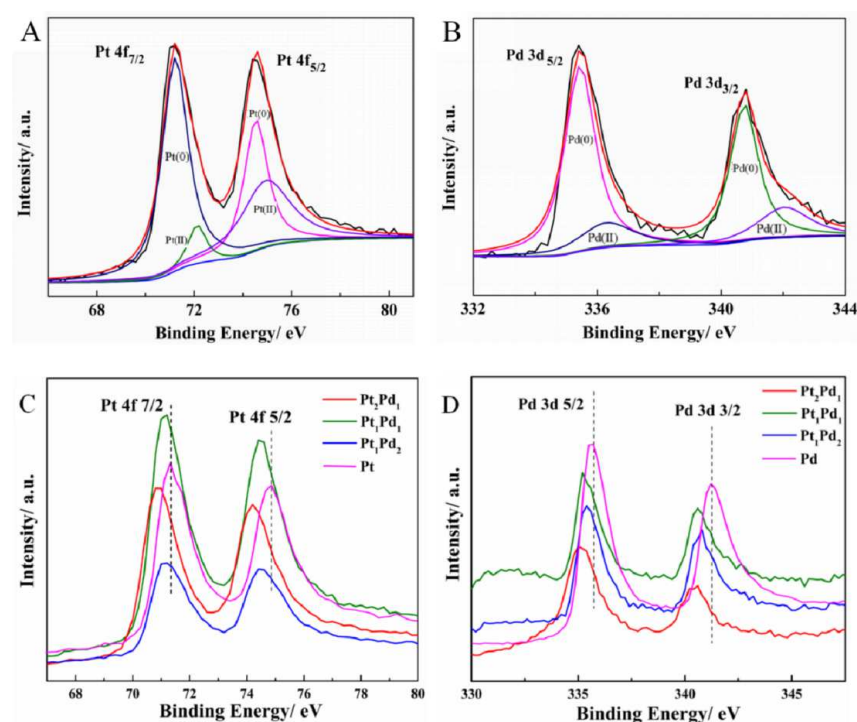


Figure 3. XPS spectra of (A) Pt 4f, (B) Pd 3d of Pt₁Pd₂ NCs; and (C) Pt 4f; (D) Pd 3d of Pt NCs, Pt₂Pd₁ NCs, Pt₁Pd₁ NCs, Pt₁Pd₂ NCs, and Pd NCs.

3.2. Electrochemical Characterization

Simultaneously, the electrocatalytic ability of PtPd NCs/MWCNT catalysts for methanol oxidation is studied and compared with the commercial Pd/C catalyst (JM) and the commercial Pt/C catalyst (JM). Figure 4A is a cyclic voltammogram of Pt₁Pd₁ NCs/MWCNTs, Pt₂Pd₁ NCs/MWCNTs, Pt₁Pd₂ NCs/MWCNTs, Pd/C (JM), and Pt/C (JM) catalysts in 0.5 M KOH + 2.0 M CH₃OH solution. It can be seen from Figure 4A that the peak current is located at about 0.9 V in the forward scan, which is usually the oxidation current of the C-H bond splitting during methanol oxidation. In reverse scanning peak current is attributed to the oxidation species formed on the catalyst surface in the CV curve, which is about 0.8 V during the reverse scan. In the forward scan, the Pt₁Pd₂ NCs/MWCNT catalyst showed the highest current density (658.5 mA · mg^{−1}) of all these synthesis catalysts, which was 1.5-times the commercial Pt/C (436 mA · mg^{−1}) and 3.9-times the commercial Pd/C (169 mA · mg^{−1}). At the same time, Pt₁Pd₁-NCs/MWCNT and Pt₂Pd₁-CNS/MWCNT catalysts are also higher than commercial Pd/C catalysts and commercial Pt/C catalysts. The high electrocatalytic activity of PtPd NCs/MWPNT catalysts for methanol oxidation may be attributed to the synergistic effect between Pt and Pd atoms. The high catalytic activity of the Pt₁Pd₂-NCs/MUCNT catalyst while reducing the Pt content is related to more active sites being exposed by the smaller diameter of Pt₁Pd₂ NCs/MWCNT nanochains. In reverse scanning, the peak current density of the Pt₁Pd₂-NCs/MWCNT catalyst is still higher than that of Pt₁Pd₂ NCs/MWCNT, Pt₂Pd₁-NCs/MWPNT, Pt/C, and Pd/C catalysts, which indicates that the Pt₁Pb₂-NCs/MWCET catalyst has good reversibility of oxygen adsorption and desorption [32]. In addition, we compared the catalysts reported in other studies for methanol fuel cells and the corresponding comparisons are listed in Table 2. It shows that PtPd NCs/MWCNT catalysts are superior to many other reported electrocatalysts [33–37].

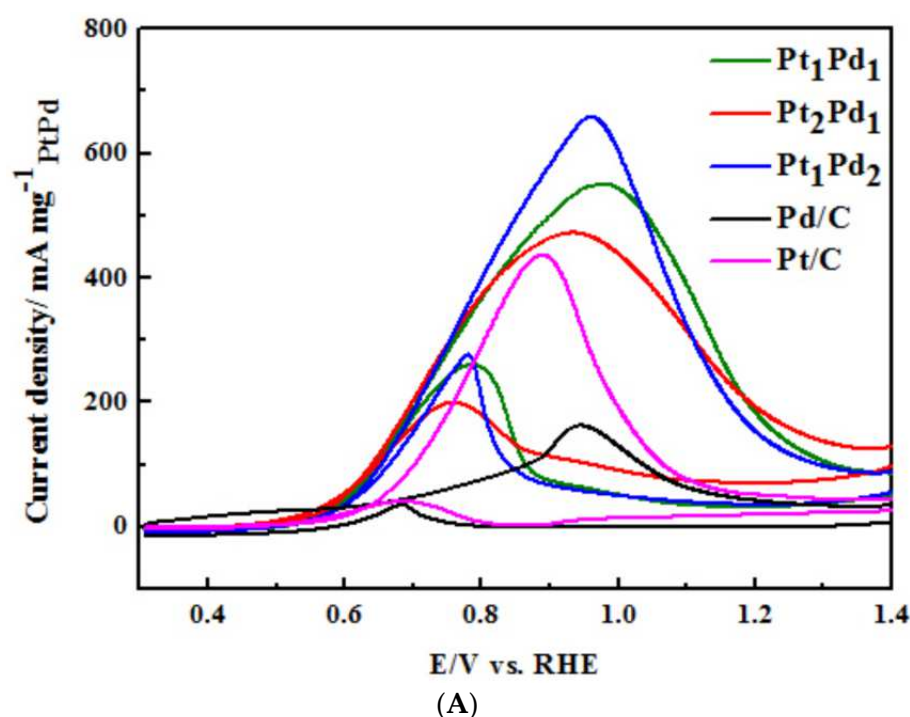


Figure 4. Cont.

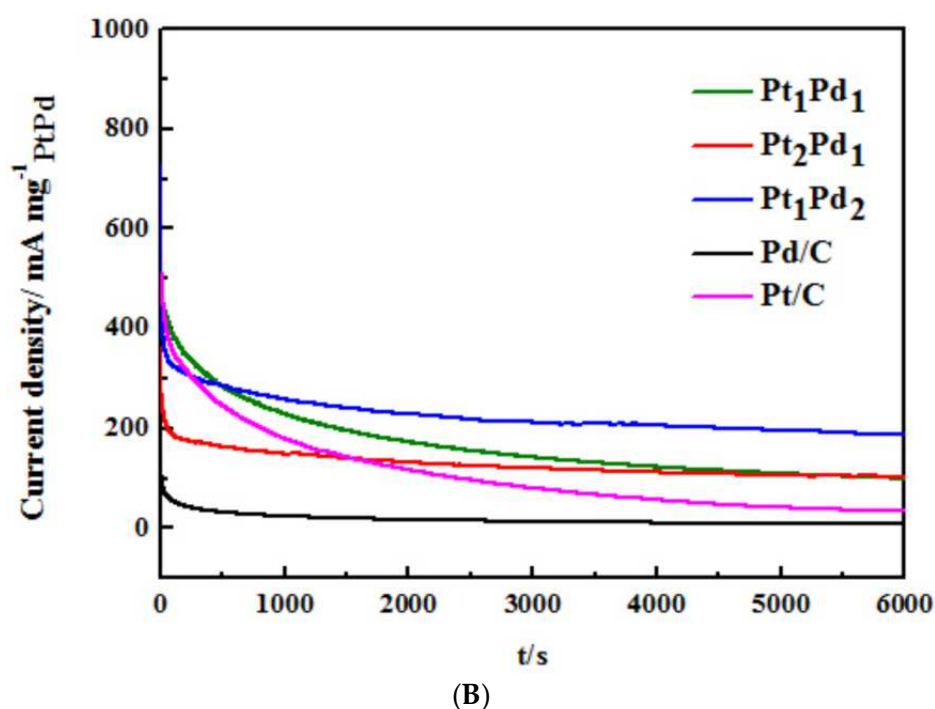
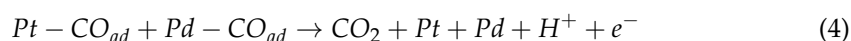
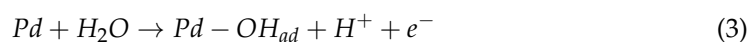
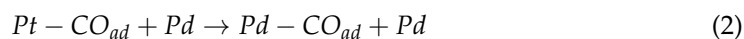
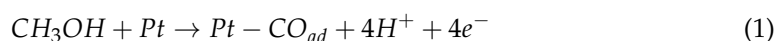


Figure 4. (A) CV, (B) *i*-*t* curves of Pt₂Pd₁ NCs/MWCNTs, Pt₁Pd₁ NCs/MWCNTs, Pt₁Pd₂ NCs/MWCNTs and the commercial Pd/C catalysts in a solution containing 0.5 M KOH + 2.0 M CH₃OH.

Table 2. The compared electrochemical performance of PtPd NCs/MWCNTs with the other reported Pd-based catalysts for methanol oxidation.

Catalysts	Electrolytes	Scan Rate (mV·s ⁻¹)	Current (mA·mg ⁻¹ _{Pd})	Ref.
Pd/NS-G	0.5 M NaOH + 1.0 M Methanol	50	399	[34]
Nanoporous Pd/NiO	0.5 M NaOH + 0.5 M Methanol	50	344	[35]
Pt-MnO ₂ /MWCNTs	0.5 M NaOH + 1.0 M Methanol	50	431	[36]
YS Pd-Ni-P/C	0.5 M KOH + 1.0 M Methanol	50	524	[37]
Pt ₅₀ Pd ₅₀ /SCs	1.0 M KOH + 1.0 M Methanol	50	336	[38]
Pt ₂ Pd ₁ /MWCNTs	0.5 M KOH + 2.0 M Methanol	50	472	This work
Pt ₁ Pd ₁ /MWCNTs	0.5 M KOH + 2.0 M Methanol	50	531	This work
Pt ₁ Pd ₂ /MWCNTs	0.5 M KOH + 2.0 M Methanol	50	685	This work

The synergistic effect of the PtPd alloy can not only promote the oxidation of adsorbed intermediate oxygen species at low potential, but also improve the anti-poisoning ability of the catalyst. In the reaction process, *Pt* occupies the main dehydrogenation site and *Pd* accelerates the removal of CO, thereby inhibiting the poisoning of *Pt*. The mechanism of the reaction is summarized as follows [38]:



The stability of the catalyst is a critical issue for the lifetime of DMFCs. Therefore, the amperometric *i*-*t* curve is employed to compare the stability of these catalysts, including

the above two commercial catalysts. The current density of the Pt₁Pd₂ NCs/MWCNT catalyst shows the slowest decay among the three synthesized catalysts, as shown in Figure 4B, and it may be attributed to the synergistic effect of the alloy formed by different ratios of Pt and Pd, which produces different removal capacity of CO-like intermediates in methanol oxidation. The highest current density throughout the test indicated that Pt₁Pd₂ NCs/MWCNTs have the best stability and catalytic activity for methanol electrooxidation. According to the aforementioned electrochemical test results, PtPd has a distinctive network structure, a bigger specific surface area, and more active sites, which improves the electro-catalytic activity of the catalysts. Therefore, modifying the morphology by using the structure-directing agent KBr is crucial for enhancing the catalytic activity.

4. Conclusions

In this paper, a simple and effective one-step chemical reduction method is used to synthesize different molar ratios of bimetallic PtPd NC/MWCNT catalysts, with high catalytic activity and very good stability for methanol oxidation. The Pt₁Pd₂NCs/MWCNT catalyst has the highest electro-catalytic activity, 1.5-times that of the commercial Pt/C and 3.9-times that of the commercial Pd/C catalyst. It has better electro-catalytic stability than the commercial Pt/C and the commercial Pd/C catalysts. With the structure-directing agent KBr, PtPd NCs form a network structure with rough surface defects, which is beneficial to improve the catalytic activity and stability of the catalyst. In addition, Pt and Pd form the PtPd alloy structure and the intermediate species absorbed on the surface of the catalyst are more easily activated due to the interaction of the electrons between Pt and Pd atoms.

Author Contributions: Data curation, D.Z.; Investigation, Y.R.; Methodology, M.X.; Resources, Y.D. and J.Y.; Supervision, Z.J. and J.Y.; Writing—original draft, D.Z.; Writing—review & editing, J.Y. All authors have read and agreed to the published version of the manuscript.

Funding: This work was financially supported by the National Natural Science Foundation of China (No. 51764030), the Major Special Project of Yunnan Province (202102AB080007), the Natural Science Foundation of Yunnan Province (202001AS070010), and the Analysis and Testing Foundation of Kunming University of Science and Technology.

Institutional Review Board Statement: Not applicable.

Informed Consent Statement: Not applicable.

Data Availability Statement: Not applicable.

Conflicts of Interest: The authors declare no conflict of interest.

References

1. Xu, M.; Zhang, W.; Qu, Y.; Liu, X.; Zhai, C.; Liu, Y. The extended Stöber method for synthesizing nitrogen-doped porous carbon nanospheres supported Pt nanoparticles towards methanol oxidation in alkaline media. *Mater. Lett.* **2022**, *325*, 132894. [\[CrossRef\]](#)
2. Yuan, Q.; Duan, D.; Ma, Y.; Wei, G.; Zhang, Z.; Hao, X.; Liu, S. Performance of nano-nickel core wrapped with Pt crystalline thin film for methanol electro-oxidation. *J. Power Sources* **2014**, *245*, 886–891. [\[CrossRef\]](#)
3. Li, Z.; Jiang, X.; Wang, X.; Hu, J.; Liu, Y.; Fu, G.; Tang, Y. Concave PtCo nanocrosses for methanol oxidation reaction. *Appl. Catal. B Environ.* **2020**, *277*, 119135. [\[CrossRef\]](#)
4. Yang, G.; Yang, X.; Xu, M.; Min, C.; Xiao, H.; Jiang, K.; Chen, L.; Wang, G. Multi-walled carbon nanotube modified with methylene blue under ultraviolet irradiation as a platinum catalyst support for methanol oxidation. *J. Power Sources* **2013**, *222*, 340–343. [\[CrossRef\]](#)
5. Corpuz, A.R.; Olson, T.S.; Joghee, P.; Pylypenko, S.; Dameron, A.A.; Dinh, H.N.; O'Neill, K.J.; Hurst, K.E.; Bender, G.; Gennett, T.; et al. Effect of a nitrogen-doped PtRu/carbon anode catalyst on the durability of a direct methanol fuel cell. *J. Power Sources* **2012**, *217*, 142–151. [\[CrossRef\]](#)
6. Zhang, Z.; Xin, L.; Qi, J.; Chadderton, D.J.; Li, W. Supported Pt, Pd and Au nanoparticle anode catalysts for anion-exchange membrane fuel cells with glycerol and crude glycerol fuels. *Appl. Catal. B Environ.* **2013**, *136*, 29–39. [\[CrossRef\]](#)
7. Tiwari, J.N.; Tiwari, R.N.; Singh, G.; Kim, K.S. Recent progress in the development of anode and cathode catalysts for direct methanol fuel cells. *Nano Energy* **2013**, *2*, 553–578. [\[CrossRef\]](#)
8. Chen, X.; Jiang, Y.; Sun, J.; Jin, C.; Zhang, Z. Highly active nanoporous Pt-based alloy as anode and cathode catalyst for direct methanol fuel cells. *J. Power Sources* **2014**, *267*, 212–218. [\[CrossRef\]](#)

9. Liu, J.; Wang, L.; Okejiri, F.; Luo, J.; Zhao, J.; Zhang, P.; Liu, M.; Yang, S.; Zhang, Z.; Song, W.; et al. Deep understanding of strong metal interface confinement: A journey of Pd/FeO_x catalysts. *ACS Catal.* **2020**, *10*, 8950–8959. [\[CrossRef\]](#)
10. Hong, W.; Wang, J.; Wang, E. Facile synthesis of highly active PdAu nanowire networks as self-supported electrocatalyst for ethanol electrooxidation. *ACS Appl. Mater. Interfaces* **2014**, *6*, 9481–9487. [\[CrossRef\]](#)
11. Kim, Y.; Kim, H.; Kim, W.B. PtAg nanotubes for electrooxidation of ethylene glycol and glycerol in alkaline media. *Electrochem. Commun.* **2014**, *46*, 36–39. [\[CrossRef\]](#)
12. Huang, L.; Han, Y.; Zhang, X.; Fang, Y.; Dong, S. One-step synthesis of ultrathin Pt x Pb nerve-like nanowires as robust catalysts for enhanced methanol electrooxidation. *Nanoscale* **2017**, *9*, 201–207. [\[CrossRef\]](#) [\[PubMed\]](#)
13. Hosseini, M.G.; Mahmoodi, R.; Daneshvari-Esfahlan, V. Ni@ Pd core-shell nanostructure supported on multi-walled carbon nanotubes as efficient anode nanocatalysts for direct methanol fuel cells with membrane electrode assembly prepared by catalyst coated membrane method. *Energy* **2018**, *161*, 1074–1084. [\[CrossRef\]](#)
14. Tang, J.X.; Chen, Q.S.; You, L.X.; Liao, H.G.; Sun, S.G.; Zhou, S.G.; Xu, Z.N.; Chen, Y.M.; Guo, G.C. Screw-like PdPt nanowires as highly efficient electrocatalysts for methanol and ethylene glycol oxidation. *J. Mater. Chem. A* **2018**, *6*, 2327–2336. [\[CrossRef\]](#)
15. Sha, R.; Vishnu, N.; Badhulika, S. Bimetallic Pt-Pd nanostructures supported on MoS₂ as an ultra-high performance electrocatalyst for methanol oxidation and nonenzymatic determination of hydrogen peroxide. *Microchim. Acta* **2018**, *185*, 399. [\[CrossRef\]](#)
16. Cui, Z.; Hu, J.; Jiang, X.; Zhang, D.; Fang, C. Asymmetric Au/(PdAg alloy) nano-allium giganteums for their enhanced electrocatalytic performances to ethanol oxidation reaction. *J. Alloy. Compd.* **2021**, *855*, 157385. [\[CrossRef\]](#)
17. Kakade, B.A.; Tamaki, T.; Ohashi, H.; Yamaguchi, T. Highly active bimetallic PdPt and CoPt nanocrystals for methanol electro-oxidation. *J. Phys. Chem. C* **2012**, *116*, 7464–7470. [\[CrossRef\]](#)
18. Li, S.S.; Yu, J.; Hu, Y.Y.; Wang, A.J.; Chen, J.R.; Feng, J.J. Simple synthesis of hollow Pt–Pd nanospheres supported on reduced graphene oxide for enhanced methanol electrooxidation. *J. Power Sources* **2014**, *254*, 119–125. [\[CrossRef\]](#)
19. Lu, Y.; Jiang, Y.; Chen, W. Graphene nanosheet-tailored PtPd concave nanocubes with enhanced electrocatalytic activity and durability for methanol oxidation. *Nanoscale* **2014**, *6*, 3309–3315. [\[CrossRef\]](#)
20. Shahrokhian, S.; Rezaee, S. Vertically standing Cu₂O nanosheets promoted flower-like PtPd nanostructures supported on reduced graphene oxide for methanol electro-oxidation. *Electrochim. Acta* **2018**, *259*, 36–47. [\[CrossRef\]](#)
21. Lu, Y.; Jiang, Y.; Wu, H.; Chen, W. Nano-PtPd cubes on graphene exhibit enhanced activity and durability in methanol electrooxidation after CO stripping-cleaning. *J. Phys. Chem. C* **2013**, *117*, 2926–2938. [\[CrossRef\]](#)
22. Lu, Y.; Jiang, Y.; Chen, W. PtPd porous nanorods with enhanced electrocatalytic activity and durability for oxygen reduction reaction. *Nano Energy* **2013**, *2*, 836–844. [\[CrossRef\]](#)
23. Zhang, C.; Zhang, R.; Li, L.; Li, X.; Chen, W. Oxygen Electroreduction by Single PtPd Nanocubes Encaged in Hollow Carbon Nanospheres: Improved Durability and Strong Effect of Carbon-Shell Thickness. *Part. Part. Syst. Charact.* **2017**, *34*, 1700034. [\[CrossRef\]](#)
24. Zhu, C.; Guo, S.; Dong, S. Facile synthesis of trimetallic AuPtPd alloy nanowires and their catalysis for ethanol electrooxidation. *J. Mater. Chem.* **2012**, *22*, 14851–14855. [\[CrossRef\]](#)
25. Achari, I.; Dimitrov, N. Ultrathin film Pt_xPd (1-x) alloy catalysts for formic acid oxidation synthesized by surface limited redox replacement of underpotentially deposited H monolayer. *Electrochem* **2020**, *1*, 4–19. [\[CrossRef\]](#)
26. Li, S.S.; Lv, J.J.; Hu, Y.Y.; Zheng, J.N.; Chen, J.R.; Wang, A.J.; Feng, J.J. Facile synthesis of porous Pt–Pd nanospheres supported on reduced graphene oxide nanosheets for enhanced methanol electrooxidation. *J. Power Sources* **2014**, *247*, 213–218. [\[CrossRef\]](#)
27. Zhang, L.Y.; Wu, D.; Gong, Y.; Liu, H.; Chen, W.; Bi, L. Carbon Monoxide-Templated Synthesis of Coral-Like Clean PtPd Nanochains as Efficient Oxygen Reduction Catalyst. *ChemElectroChem* **2018**, *5*, 2403–2408. [\[CrossRef\]](#)
28. Suzuki, H.; Kimura, T.; Yamamoto, G.; Hashida, T.; Motomiya, K.; Tohji, K.; Sato, Y. Influence of supported PtPd nanoparticles on the tensile strength of individual multi-walled carbon nanotubes: Strength decrease by the interaction of metal and nanotube. *RSC Adv.* **2017**, *7*, 49917–49922. [\[CrossRef\]](#)
29. Bharti, A.; Cheruvally, G. Surfactant assisted synthesis of Pt-Pd/MWCNT and evaluation as cathode catalyst for proton exchange membrane fuel cell. *Int. J. Hydrogen Energy* **2018**, *43*, 14729–14741. [\[CrossRef\]](#)
30. Jin, Z.; Ji, J.; He, Q.; Yang, X.; Zhang, Y.; Xu, M. The enhanced electro-catalytic performance of Au@ Pd nanoparticles self-assembled on fluorine-modified multi-walled carbon nanotubes for methanol oxidation. *Catal. Lett.* **2018**, *148*, 3281–3291. [\[CrossRef\]](#)
31. Chu, Y.Y.; Wang, Z.B.; Cao, J.; Gu, D.M.; Yin, G.P. Ultrahigh durable PtPd/C nanowire networks catalyst synthesized by modified phase transfer method for methanol oxidation. *Fuel Cells* **2013**, *13*, 380–386. [\[CrossRef\]](#)
32. Zhao, Y.; Li, X.; Schechter, J.M.; Yang, Y. Revisiting the oxidation peak in the cathodic scan of the cyclic voltammogram of alcohol oxidation on noble metal electrodes. *RSC Adv.* **2016**, *6*, 5384–5390. [\[CrossRef\]](#)
33. Zhang, X.; Zhu, J.; Tiwary, C.S.; Ma, Z.; Huang, H.; Zhang, J.; Lu, Z.; Huang, W.; Wu, Y. Palladium nanoparticles supported on nitrogen and sulfur dual-doped graphene as highly active electrocatalysts for formic acid and methanol oxidation. *ACS Appl. Mater. Interfaces* **2016**, *8*, 10858–10865. [\[CrossRef\]](#) [\[PubMed\]](#)
34. Song, Y.; Zhang, X.; Yang, S.; Wei, X.; Sun, Z. Electrocatalytic performance for methanol oxidation on nanoporous Pd/NiO composites prepared by one-step dealloying. *Fuel* **2016**, *181*, 269–276. [\[CrossRef\]](#)
35. Zhao, Y.; Zhan, L.; Tian, J.; Nie, S.; Ning, Z. MnO₂ modified multi-walled carbon nanotubes supported Pd nanoparticles for methanol electro-oxidation in alkaline media. *Int. J. Hydrogen Energy* **2010**, *35*, 10522–10526. [\[CrossRef\]](#)

-
36. Kang, Z.; Zhao, M.; Wu, Y.; Xia, T.; Cao, J.P.; Cai, W.; Chen, L. Facial fabrication of yolk-shell Pd-Ni-P alloy with mesoporous structure as an advanced catalyst for methanol electro-oxidation. *Appl. Surf. Sci.* **2019**, *484*, 441–445. [[CrossRef](#)]
 37. Zhou, L.N.; Zhang, X.T.; Wang, Z.H.; Guo, S.; Li, Y.J. Cubic superstructures composed of PtPd alloy nanocubes and their enhanced electrocatalysis for methanol oxidation. *Chem. Commun.* **2016**, *52*, 12737–12740. [[CrossRef](#)]
 38. Ensafi, A.A.; Jafari-Asl, M.; Rezaei, B.; Abarghoui, M.M.; Farrokhpour, H. Facile synthesis of Pt-Pd@Silicon nanostructure as an advanced electrocatalyst for direct methanol fuel cells. *J. Power Sources* **2015**, *282*, 452–461. [[CrossRef](#)]